






Subcortical and hippocampal brain segmentation in 5-year-old children: Validation of FSL-FIRST and FreeSurfer against manual segmentation

Kristian Lidauer¹  | Elmo P. Pulli^{1,2}  | Anni Copeland^{1,2}  | Eero Silver^{1,2}  |
 Venla Kumpulainen¹ | Niloofar Hashempour¹ | Harri Merisaari^{1,3}  |
 Jani Saunavaara⁴ | Riitta Parkkola^{3,5} | Tuire Lähdesmäki⁶ |
 Ekaterina Saukko⁵ | Saara Nolvi^{1,7,8} | Eeva-Leena Kataja¹ |
 Linnea Karlsson^{1,2,9} | Hasse Karlsson^{1,2,9} | Jetro J. Tuulari^{1,2,10,11}

¹FinnBrain Birth Cohort Study, Turku Brain and Mind Center, Department of Clinical Medicine, University of Turku, Turku, Finland

²Department of Psychiatry, Turku University Hospital, University of Turku, Turku, Finland

³Department of Radiology, University of Turku, Turku, Finland

⁴Department of Medical Physics, Turku University Hospital, Turku, Finland

⁵Department of Radiology, Turku University Hospital, Turku, Finland

⁶Department of Paediatric Neurology, Turku University Hospital and University of Turku, Turku, Finland

⁷Turku Institute for Advanced Studies, University of Turku, Turku, Finland

⁸Department of Psychology and Speech-Language Pathology, University of Turku, Turku, Finland

⁹Centre for Population Health Research, University of Turku and Turku University Hospital, Turku, Finland

¹⁰Turku Collegium for Science, Medicine and Technology, University of Turku, Turku, Finland

¹¹Department of Psychiatry, University of Oxford, UK (Sigrid Juselius Fellowship), Oxford, UK

Correspondence

Kristian Lidauer, FinnBrain Birth Cohort Study, Turku Brain and Mind Center, Department of Clinical Medicine, University of Turku, Teutori building 2nd floor, Lemminkäisenkatu 3, 21520 Turku, Finland.
 Email: kjlida@utu.fi

Funding information

National Alliance for Research on Schizophrenia and Depression, Grant/

Abstract

Developing accurate subcortical volumetric quantification tools is crucial for neurodevelopmental studies, as they could reduce the need for challenging and time-consuming manual segmentation. In this study, the accuracy of two automated segmentation tools, FSL-FIRST (with three different boundary correction settings) and FreeSurfer, were compared against manual segmentation of the hippocampus and subcortical nuclei, including the amygdala, thalamus,

Abbreviations: AAM, active appearance model; ADHD, attention deficit hyperactivity disorder; DSC, Dice score coefficient; DTI, diffusion tensor imaging; FOV, field of view; GP, globus pallidus; GRAPPA, generalised autocalibrating partially parallel acquisition; ICC, intraclass correlation coefficient; MR, magnetic resonance; MRI, magnetic resonance image; PAT, parallel acquisition technique; PCC, Pearson correlation coefficient; PTSD, post-traumatic stress disorder; SD, standard deviation; TE, time to echo; TI, inversion time; TR, repetition time; TSE, turbo spin echo.

Kristian Lidauer and Elmo P. Pulli shared contribution.

This is an open access article under the terms of the [Creative Commons Attribution-NonCommercial-NoDerivs](https://creativecommons.org/licenses/by-nc-nd/4.0/) License, which permits use and distribution in any medium, provided the original work is properly cited, the use is non-commercial and no modifications or adaptations are made.

© 2022 The Authors. *European Journal of Neuroscience* published by Federation of European Neuroscience Societies and John Wiley & Sons Ltd.

Award Number: 1956; Suomen Aivosäätiö; Sigrid Jusélius Foundation; Alfred Kordelin Foundation; Emil Aaltonen Foundation; State Grants for Clinical Research; Turku University Foundation; Hospital District of Southwest Finland; State Grants for Clinical Research; Academy of Finland, Grant/Award Number: 325292; State Grants for Clinical Research (ERVA); Brain and Behavior Research Foundation; Hospital District of Southwest Finland; University of Turku Graduate School; Orion Research Foundation; Lastenlinnan säätiö; Finnish Cultural Foundation; Turunmaan Duodecim-seura; Finnish Brain Foundation; Juho Vainio Foundation; Päivikki and Sakari Sohlberg Foundation

Edited by: John Foxe

putamen, globus pallidus, caudate and nucleus accumbens, using volumetric and correlation analyses in 80 5-year-olds.

Both FSL-FIRST and FreeSurfer overestimated the volume on all structures except the caudate, and the accuracy varied depending on the structure. Small structures such as the amygdala and nucleus accumbens, which are visually difficult to distinguish, produced significant overestimations and weaker correlations with all automated methods. Larger and more readily distinguishable structures such as the caudate and putamen produced notably lower overestimations and stronger correlations. Overall, the segmentations performed by FSL-FIRST's default pipeline were the most accurate, whereas FreeSurfer's results were weaker across the structures.

In line with prior studies, the accuracy of automated segmentation tools was imperfect with respect to manually defined structures. However, apart from amygdala and nucleus accumbens, FSL-FIRST's agreement could be considered satisfactory (Pearson correlation > 0.74 , intraclass correlation coefficient (ICC) > 0.68 and Dice score coefficient (DSC) > 0.87) with highest values for the striatal structures (putamen, globus pallidus, caudate) (Pearson correlation > 0.77 , ICC > 0.87 and DSC > 0.88 , respectively). Overall, automated segmentation tools do not always provide satisfactory results, and careful visual inspection of the automated segmentations is strongly advised.

KEYWORDS

brain, brain (growth and development), child, neuroimaging

1 | INTRODUCTION

The hippocampus and subcortical structures (henceforth collectively referred to as subcortical structures) of the brain are responsible for numerous important functions. The hippocampus and the amygdala, located in the medial temporal lobe, form an important part of the limbic system. The hippocampus has a significant role in the memory forming process (McDonald & Mott, 2017; Sawangjit et al., 2018) and has been linked to many psychopathologies such as post-traumatic stress disorder (PTSD) and Alzheimer's disease (Fitzgerald et al., 2019; Jaroudi et al., 2017). The amygdala has an important role in emotional responses, especially fear (Krabbe et al., 2018). It has also been associated with anxiety disorders and depression (Ferri et al., 2018; Toazza et al., 2016; Tye et al., 2011). The thalamus, also a part of the limbic system, relays sensory and motor signals to the cerebral cortex and regulates sleep, consciousness and alertness, among other functions. Structural changes of the thalamus have been associated with many neurological diseases such as Alzheimer's disease (Braak & Braak, 1991) and schizophrenia (Parnaudeau et al., 2018). Parts of the basal ganglia, including the

putamen, the globus pallidus (GP), the caudate nucleus and the nucleus accumbens, have an important role in the extrapyramidal motor system and are associated with many motor neurodegenerative pathologies such as Huntington's and Parkinson's disease (Manes et al., 2018; Singh-bains et al., 2016). In addition, they are involved in motivational, emotional and cognitive functions (Herrero & Barcia, 2002). The development of these subcortical structures can be affected by early-life environments and experiences (Lee et al., 2019; Pulli et al., 2019). Taken together, the subcortical areas are relevant to multiple brain functions and pathologies. Therefore, it is also crucial to gather accurate information about them in magnetic resonance imaging (MRI) studies conducted in paediatric populations.

Accurate segmentation of paediatric MR images is challenging, partly due to the variation in pre-processing and segmentation protocols (Hashempour et al., 2019; Schoemaker et al., 2016). Several segmentation protocols have been developed for adult brains, but they cannot be directly applied in segmenting child brain images because children's MR images have different contrast and comparatively lower resolution than adults' images (Gousias et al., 2012; Moore et al., 2014; Morey

et al., 2009). Manual segmentation is currently considered the gold standard in volumetric segmentation. Although it is considered the most accurate method, it is highly time consuming and requires expertise for adequate results. Furthermore, a major downside is the subjective approach in estimating the shapes and sizes of the structures, which may cause reproducibility issues that may be even more pronounced in larger samples.

Several software have been developed for automated segmentation of the brain. In this study, we focused on two mainstream analysis pipelines. One is FSL-FIRST from the FMRIB Software Library (Patenaude et al., 2011). FSL-FIRST is a segmentation tool that uses the template based on manually segmented images to construct the shape of the automated segmentation models. It utilises the active appearance model (AAM) combined with a Bayesian framework, which allows probabilistic relationships between voxel intensity and the shapes of different structures (Patenaude et al., 2011). The other is FreeSurfer (<https://surfer.nmr.mgh.harvard.edu/>), which is an open-source software suite for processing and analysing MR images. FreeSurfer uses a five-stage volume-based stream for segmenting subcortical structures. Final segmentation is based on a subject-independent probabilistic atlas and subject specific values. Both FSL-FIRST and FreeSurfer use a training dataset for the basis of segmentation and utilise probabilistic computing to determine the final shape and volume of each structure. Although both FSL-FIRST and FreeSurfer were originally developed mainly for adult brain image analyses, both software have also been used in paediatric neuroimaging. There are multiple recent studies using both FSL-FIRST (Sandman et al., 2014; Wang et al., 2022) and FreeSurfer (Barch, Harms, et al., 2019; Barch, Tillman, et al., 2019; Grohs et al., 2021; Roediger et al., 2021) as a tool for paediatric volumetric subcortical brain segmentation. Majority of these studies did not use manual segmentation as a control for segmentation accuracy.

Consistent overestimation of subcortical volumes regarding both FreeSurfer and FSL-FIRST (Cherbuin et al., 2009; Doring et al., 2011) has been a common finding in previous studies. This result has been documented in paediatric populations on the hippocampus and amygdala (Mulder et al., 2014; Schoemaker et al., 2016). The study by Schoemaker et al. also found that the consistency between manual segmentation and FreeSurfer was better than between manual segmentation and FSL-FIRST in children aged between 6 and 11 years (Schoemaker et al., 2016). Although the reliability of these segmentation methods has been assessed in multiple studies in the medial temporal lobe structures, there has been little research including the striatal structures.

The aim of this study was to compare the accuracy of FSL-FIRST and FreeSurfer against the gold standard manually corrected segmentation on subcortical structures, including the hippocampus, amygdala, thalamus, putamen, GP, caudate and nucleus accumbens, in paediatric populations. Therefore, we compared the volumes of all the structures extracted from each segmentation method. Furthermore, we analysed the shape of the segmentation models to determine the areas where the automated segmentation tools overestimated or underestimated the size of the structures and their borders. This was a feasibility study that critically assessed the extent to which adult delineation software can be used to segment child brain images that have nearly adult-like contrast pattern in T1-weighted images and are close in size to adult brain.

2 | MATERIAL AND METHODS

This study was conducted in accordance with the Declaration of Helsinki, and it was approved by the Joint Ethics Committee of the University of Turku and the Hospital District of Southwest Finland (07.08.2018) §330, ETMK: 31/180/2011.

2.1 | Subjects

MRI scans were acquired in children as part of the Finn-Brain Birth Cohort Study (www.finnbrain.fi), which was started in 2011. The main goal of the cohort is to study the effects of genes and environment on the development and mental health of children (Karlsson et al., 2018). Initial recruitment of FinnBrain Birth Cohort Study was performed systematically in routine ultrasound examinations during the 12th week of gestation. At 5 years of age, 203 subjects attended neuroimaging visits. For the purposes of this study, we selected the first 80 participants that were visually confirmed to have high enough quality T1 image for manual segmentation of the subcortical structures. For the 5-year neuroimaging visit, we primarily recruited participants that had a prior visit to neuropsychological measurements at ~5 years of age ($n = 76$). This sample also includes four other subjects: Three subjects were included without a neuropsychological visit, as they had an exposure to maternal prenatal synthetic glucocorticoid treatment (recruited separately for a nested case-control sub-study). The data additionally included one subject that was enrolled for a pilot scan at the beginning of the studies. The total sample size for this study was 80. The exclusion criteria for this study were (1) born before gestational week 35 (born before gestational week

TABLE 1 Participant demographics and maternal medical history variables ($N = 80$)

Continuous variables	Mean	SD	Min	Max
Age at scan (years)	5.34	0.06	5.08	5.52
Gestational age at birth (weeks)	39.5	1.7	33.9	42.3
Birth weight (grams)	3437	557	1790	4980
Maternal age at term (years)	31.4	4.4	20.2	42.0
Maternal BMI before pregnancy	23.8	3.9	18.1	34.7
Categorical variables			Number	Per cent
Sex				
Male			46	57.5
Female			34	42.5
Maternal education level				
Upper secondary school or vocational school or lower			15	18.8
University of applied sciences			23	28.7
University			42	52.5
Maternal monthly income, estimated after taxes (euros)				
≤1500			20	25.0
1501–2500			49	61.3
2501–3500			7	8.8
≥3501			1	1.3
Missing			3	3.8
Maternal background				
Finnish			79	98.8
Other			1	1.3
Alcohol use during pregnancy				
Yes, continued to some degree after learning about pregnancy			8	10.0
Yes, stopped after learning about the pregnancy			16	28.0
No			51	63.8
Missing			5	6.3
Tobacco smoking during pregnancy				
Yes, continued to some degree after learning about pregnancy			2	2.5
Yes, stopped after learning about the pregnancy			3	3.8
No			71	88.8
Missing			4	5.0
Illicit drug use during pregnancy				
No			75	93.8
Missing			5	6.3
Maternal history of disease, yes ($N = 77$, 3 missing)				
Allergies			32	41.6
Depression			11	14.3
Asthma			9	11.7
Eating disorder			9	11.7
Chronic urinary tract infection			8	10.4
Anxiety disorder			7	9.1

(Continues)

TABLE 1 (Continued)

Categorical variables	Number	Per cent
Autoimmune disorder	5	6.5
Hypertension	3	3.9
Hypercholesterolaemia	2	2.6
Coeliac disease	2	2.6
Hypothyroidism	2	2.6
Emphysema	1	1.3
Chronic bacterial or viral infection	1	1.3
Psychosis	1	1.3
Drug dependency	1	1.3
Migraine	1	1.3
Other chronic disease	6	7.8
Maternal medication at gestational week 14, yes (<i>N</i> = 72, 8 missing)		
Thyroxin	6	8.3
Corticosteroid	4	5.6
SSRI/SNRI	3	4.2
Hypertension medication	2	2.8
Other mood medication	2	2.8
Other medication affecting the CNS	1	1.4
Other medication	6	8.3
Maternal medication at gestational week 34, yes (<i>N</i> = 75, 5 missing)		
Thyroxin	7	9.3
Blood pressure medication	5	6.7
SSRI/SNRI	4	5.3
Corticosteroid	4	5.3
Other mood medication	2	2.7
Other medication affecting the CNS	2	2.7
Other medication	14	18.7

Notes: Gestational age at birth was calculated using the difference between due date and actual date of birth. Maternal age at term was calculated as follows: The age as days at due date divided by 365.25. On the question about alcohol usage, three subjects answered that they did not use alcohol during pregnancy, but also answered that they stopped using alcohol when they learned about the pregnancy. These were classified as 'yes, stopped when learning about pregnancy'. The data for monthly income estimate, alcohol use, tobacco use, drug use and diagnostic information are from questionnaires at gestational Week 14. Maternal education level was asked in questionnaires at gestational Week 14 and at 5 years of age, and the most recent available data was used. In addition to the diseases in the table, we asked for the following disorders, and none of the mothers suffered from them: myocardial infarction, cardiac dysfunction, angina pectoris, stroke, Type 1 diabetes, Type 2 diabetes, epilepsy, intellectual disability, alcohol dependency disorder, musculoskeletal disorder, cancer and attention deficit hyperactivity disorder. Sex, birth weight, and maternal BMI before pregnancy were retrieved from the National Institute for Health and Welfare (www.thl.fi).

Abbreviations: BMI, body mass index; CNS, central nervous system; N, number of participants; SD, standard deviation; SNRI, selective noradrenalin reuptake inhibitor; SSRI, selective serotonin reuptake inhibitor.

32 in the synthetic glucocorticoid treatment group); (2) developmental anomaly or abnormalities in senses or communication (e.g. congenital heart disease, blindness and deafness); (3) known long-term medical diagnosis (e.g. epilepsy, autism and attention deficit hyperactivity disorder [ADHD]); (4) ongoing medical examinations or clinical follow-up in a hospital (meaning there has been a referral from primary care setting to experts); (5) child

use of continuous, daily medication (including per oral medications, topical creams and inhalants. One exception to this was desmopressin [[®]Minirin] medication, which was allowed); (6) history of head trauma (defined as concussion necessitating clinical follow-up in a health-care setting or worse); and (7) metallic ear tubes (to assure good-quality scans) and routine MRI contraindications.

In this study, we used a representative subsample of 80 T1-weighted brain images, which were all visually inspected by a single expert rater (Kristian Lidauer). The sample included 34 girls and 46 boys aged between 5 and 5.5 years (mean age 5.34 years, SD = 0.06). Participant demographics and maternal medical history variables are presented in detail in Table 1.

2.2 | Study visit

The subjects were recruited for the neuroimaging visits via phone calls by a research staff member. On the first call, the families were given general information about the study, and the inclusion and exclusion criteria were checked. The follow-up call was made to confirm the participation, and we gave instructions to practice for the MRI visit at home. A member of the research staff made a home visit before the scan to deliver earplugs and headphones, to give more detailed information about the visit and to answer any remaining questions. An added benefit of the home visit was the chance to meet the participating child and that way start the familiarisation with the research staff, which helped the preparations on the scanning day. A written consent was acquired from both parents before the MRI scan as well as verbal assent from the child.

Multiple methods were applied to reduce anxiety and make the visit feel as safe as possible (many of the methods have been described in earlier studies) (Greene et al., 2016). The visit was conducted in a child-friendly manner with a flexible timetable in the preparation before the scan, and we did our best to accommodate in order to benefit the child in cooperation with the family. The participants were scanned awake. During the structural imaging, the subjects were allowed to watch a cartoon or a movie of their choice. A parent and a research staff member were present in the scanner room throughout the scan. Everyone in the room had their hearing protected with earplugs and headphones. The maximum scan time was 60 min, and the subjects were allowed to stop the scan at any time. For a more detailed description of the study visits, see (Pulli et al., 2022) and (Copeland et al., 2021).

2.3 | MRI acquisition

Participants were scanned using a Siemens Magnetom Skyra fit 3 T with a 20-element head/neck matrix coil. We used generalised autocalibrating partially parallel acquisition (GRAPPA) technique to accelerate image acquisition [parallel acquisition technique (PAT) factor

of 2 was used]. For the purposes of the current study, we acquired a high-resolution three-dimensional (3D) T1-weighted magnetisation prepared rapid acquisition gradient-echo sequence (MPRAGE) in sagittal plane with the following sequence parameters: TR = 1900 ms, TE = 3.26 ms, TI = 900 ms, flip angle = 9°, voxel size = 1.0 × 1.0 × 1.0 mm³, FOV = 256 mm. In addition, the max. 60-min scanning protocol included a T2 turbo spin echo (TSE), a 7-min resting state functional MRI and a DTI sequence. The T1 scans were planned as per recommendations of the FreeSurfer developers (https://surfer.nmr.mgh.harvard.edu/fswiki/FreeSurferWiki?action=AttachFile&do=get&target=FreeSurfer_Suggested_Morphometry_Protocols.pdf, at the time of writing).

2.4 | Automated segmentation of the subcortical nuclei using FSL-FIRST

The automated segmentation of the subcortical structures was performed using FSL-FIRST 5.0.9 (Patenaude et al., 2011), a freely available automated segmentation tool provided by the FMRIB Software Library. FSL-FIRST uses a training data-based approach combined with a Bayesian probabilistic model to determine the most probable shape of the structure given the intensities of the T1 image. FSL-FIRST makes use of the adult MNI152 template space, but the segmentation model has been trained structures using 336 manually labelled T1-weighted MR images (age range 4.7–87 years) (Patenaude et al., 2011). More detailed information about the technical process can be found in an article by Patenaude et al. (2011). In this study, we segmented the T1 images using FSL-FIRST with three different boundary correction settings. The *FSL Default* method uses different options based on empirical observations for each different structure. The *FSL Fast* option uses an FSL-FAST-based tissue-type classification to determine the final shape of the model. For the third boundary correction option, we chose *FSL None*, which does not use any boundary correction settings. After running the pipelines, a voxel count was performed to estimate the volumes produced by each different method.

2.5 | Automated segmentation of the subcortical nuclei using FreeSurfer

The other automated segmentation software used in this study was FreeSurfer 6.0 (<https://surfer.nmr.mgh.harvard.edu/>), a freely available open software neuro-image analysis suite. We used the recon-all pipeline with

default settings consisting of several stages. In brief, the process includes motion correcting and averaging (Reuter et al., 2010) of multiple T1 images, which is preceded by removal of non-brain tissue using a watershed/surface deformation procedure (Segonne et al., 2004), after which the images are transferred into a Talairach space, where the white matter and subcortical grey matter are segmented by labelling each voxel based on the probabilities from a manually edited training dataset and the intensities of the T1 image. FreeSurfer segmentation labels via probabilistic information automatically estimated from expert segmentations of 40 adult brain images (Fischl et al., 2002) (<https://surfer.nmr.mgh.harvard.edu/fswiki/FreeSurferMethodsCitation>). FreeSurfer morphometric procedures have been demonstrated to show good test-retest reliability across scanner manufactures and across field strengths (Reuter et al., 2012). The technical details of the FreeSurfer process are described more in-depth in prior publications (Fischl et al., 2002, 2004; Segonne et al., 2004). The volumes were extracted with 'asegstats2table' command.

2.6 | Manual segmentation of the subcortical nuclei

Manual segmentation was done by editing the models produced by *FSL None*. We visually inspected the results of all three FSL-FIRST pipelines and chose *FSL None*, because it required the least amount of editing. The subcortical structures were segmented by a single expert rater (Kristian Lidauer) using the software FslView (<https://fsl.fmrib.ox.ac.uk/fsl/fslwiki/FslView>). The rater was experienced in manual segmentation of infant brain MR images and templates (Acosta et al., 2020; Hashempour et al., 2019) across a period of 2 years before starting the current study (2018–2020).

The use of initial estimates from FSL-FIRST significantly reduced the working time as compared with full manual segmentation. It also made the work easier as the main task for the investigators was correction of the borders. This process was guided by prior work for striatal structures (Perlaki et al., 2017) and the thalamus (Owens-Walton et al., 2019; Power et al., 2015) as well as our prior work for amygdala and hippocampus segmentation, which is provided in our recent open-access article (Hashempour et al., 2019).

The manual edits were performed on 'initial estimates' that saved time. The edits were documented on 40 randomly chosen subjects of the total 80 to highlight important areas for quality control. The anatomical delineations that we incorporated into locally adapted procedures are in line with prior work (de Macedo Rodrigues

et al., 2015). Manual segmentations/edits were performed in a slice-by-slice manner to carefully trace the correct anatomical border and reviewed in axial, coronal and sagittal planes for a 3D consistency of the segmentations. Finally, all segmentations were checked for accuracy by senior scientist (Jetro J. Tuulari). The accuracy check was performed with fsleyes and entailed (1) selection of a reference segmentation with all structures accurately delineated, (2) opening three segmentations at a time and comparing them against the reference segmentation, (3) checking bilateral structures from each one by browsing the structure in all 3D planes and checking the borders with intermittent opening and closing the overlay to check the consistency of the borders. This process took about 15 min per three segmentation (~7 h in the final round of quality control).

To assess any bias that might occur with FSL-FIRST-based initial estimates, we re-segmented 20 randomly chosen subjects using automated FreeSurfer segmentations as the base for manual delineation. We also re-segmented 10 randomly chosen subjects using FSL-FIRST *None* initial estimates to assess intra-rater accuracy.

A voxel count was then concluded with fslmaths to estimate the volumes of the manually segmented structures.

2.7 | Statistical analysis

All statistical analyses and plotting of the results were performed using R tools v.4.0 (<https://www.r-project.org/>) and R-Studio 1.3 (<https://rstudio.com/>). For the plots and following analyses, we used irr, ggplot2, gridExtra, grid and gtable libraries.

The volumetric difference between automated segmentation and manual segmentation was calculated as the percentage using the following equation (Schoemaker et al., 2016): $\%VD = [(V_a - V_m)/V_m] \times 100\%$, where V_a is the automated volume and V_m is the manually segmented volume. A negative result indicates that the automated method underestimated the volume, whereas a positive value shows that the automated method overestimated the volume.

Pearson correlations were calculated to measure the strength of the association between manual segmentation and the different automated techniques for each individual structure. A strong correlation would indicate good consistency between methods. To estimate reproducibility between different techniques and estimation bias, we computed intraclass correlation coefficients (ICC). We used a two-way mixed effect model with absolute agreement and average measures (ICC Type A, k) as specified

TABLE 2 Comparison of mean (standard deviation) volumes and percentage of volume difference between techniques

	Manual	FSL-FIRST			FreeSurfer
		Default	Fast	None	
Volume (SD)					
L-hippocampus	3019.89 (444.14)	3412.41 (441.28)	3412.41 (441.28)	4244.95 (575.67)	4076.74 (384.19)
R-hippocampus	3150.08 (425.61)	3551.45 (415.35)	3551.45 (415.35)	4434.70 (531.64)	4189.92 (393.52)
L-amygdala	892.89 (169.80)	1096.85 (203.91)	1096.85 (203.91)	1377.63 (232.26)	1540.28 (214.03)
R-amygdala	845.36 (174.28)	1053.94 (194.49)	1053.94 (194.49)	1306.54 (228.94)	1734.00 (193.02)
L-thalamus	7354.33 (723.20)	8194.63 (665.97)	6713.21 (547.86)	8194.63 (665.97)	7751.61 (565.98)
R-thalamus	7274.78 (691.27)	8053.54 (653.88)	6612.65 (528.49)	8053.54 (653.88)	7714.82 (577.31)
L-putamen	4899.50 (508.16)	5152.74 (509.74)	4695.56 (482.28)	5152.74 (509.74)	5178.54 (570.61)
R-putamen	4924.40 (530.36)	5250.24 (541.97)	4656.94 (501.47)	5250.24 (541.97)	5283.99 (580.31)
L-GP	1644.91 (159.43)	1775.01 (152.92)	1377.19 (150.87)	1775.01 (152.92)	2064.27 (241.91)
R-GP	1664.09 (171.18)	1780.10 (165.80)	1348.86 (153.55)	1780.10 (165.80)	1938.86 (188.74)
L-caudate	4018.88 (428.88)	3870.68 (441.35)	3870.68 (441.35)	5014.68 (577.25)	3931.77 (426.83)
R-caudate	4222.35 (464.31)	4016.30 (511.14)	4016.30 (511.14)	5059.09 (643.09)	4052.67 (419.55)
L-accumbens	523.96 (100.67)	610.65 (128.79)	610.65 (128.79)	804.31 (136.64)	568.37 (114.45)
R-accumbens	428.64 (86.09)	534.33 (96.44)	534.33 (96.44)	675.84 (117.69)	635.72 (97.09)
L-cau + acc	4542.85 (469.18)	4481.33 (497.87)	4481.33 (497.87)	5818.99 (641.97)	4500.13 (484.39)
R-cau + acc	4650.99 (480.17)	4550.63 (531.08)	4550.63 (531.08)	5734.93 (659.63)	4688.39 (472.09)
Combined mean	3204.58	3453.78	3110.79	3794.57	3618.68
% volume diff. (SD)					
L-hippocampus		13.61 (9.31)	13.61 (9.31)	41.15 (10.62)	37.10 (20.12)
R-hippocampus		13.45 (10.27)	13.45 (10.27)	41.58 (12.75)	34.55 (16.01)
L-amygdala		24.65 (21.68)	24.65 (21.68)	56.56 (23.88)	77.02 (34.11)
R-amygdala		27.02 (22.55)	27.02 (22.55)	57.75 (27.28)	112.00 (40.58)
L-thalamus		11.73 (5.75)	-8.49 (4.43)	11.73 (5.75)	5.96 (8.72)
R-thalamus		10.93 (4.85)	-8.90 (4.06)	10.93 (4.85)	6.52 (8.08)
L-putamen		5.24 (2.06)	-4.13 (2.38)	5.24 (2.06)	5.81 (6.76)
R-putamen		6.69 (2.45)	-5.39 (2.80)	6.69 (2.45)	7.49 (6.98)
L-GP		8.08 (3.89)	-16.28 (4.28)	8.08 (3.89)	26.00 (14.00)
R-GP		7.16 (4.38)	-18.92 (4.58)	7.16 (4.38)	17.17 (12.02)
L-caudate		-3.50 (7.15)	-3.50 (7.15)	25.14 (11.12)	-1.99 (6.12)
R-caudate		-4.89 (6.49)	-4.89 (6.49)	19.91 (9.84)	-3.72 (7.00)
L-accumbens		17.58 (18.59)	17.58 (18.59)	55.34 (20.97)	10.79 (24.05)
R-accumbens		26.13 (15.34)	26.13 (15.34)	60.02 (22.24)	52.08 (27.03)
L-cau + acc		-1.17 (7.26)	-1.17 (7.26)	28.44 (10.89)	-0.80 (6.06)
R-cau + acc		-2.12 (6.31)	-2.12 (6.31)	23.47 (9.47)	1.03 (6.60)
Combined mean		11.71	3.71	29.09	27.63

Notes: The volumetric unit used is 1 voxel (= 1 mm³). Description of mean volumes obtained from each method as well as mean percentage of volume difference (% volume diff.) between manual segmentation, FreeSurfer and different FSL-FIRST pipelines.

Abbreviations: Cau + acc, combined volume of the caudate and nucleus accumbens; Combined mean, mean of all structures combined; GP, globus pallidus; L, left; R, right; SD, standard deviation.

by McGraw and Wong (1996), which is a model not defined in the commonly used Shrout and Fleiss (1979) convention. A high value would confirm a good reproducibility between two raters. There are no fixed guidelines on how to interpret ICC values, but in previous studies, a coefficient of 0.70 has been considered as the minimum for establishing an adequate reliability between two raters (Terwee et al., 2007).

To determine the spatial overlap of the structures, we conducted Dice score coefficient (DSC) analysis between manual and automated segmentation methods. The value of DSC ranges from 0, indicating no spatial overlap between structures, to 1, indicating complete overlap (Zou et al., 2004).

The same correlations and DSC were also calculated for comparison between manual segmentation based on either *FSL None* or FreeSurfer automated segmentation and between intra-rater segmentations.

To assess the adequacy of sample size, we performed a split-half analysis, where we divided the whole sample ($n = 80$) into two randomly selected subsamples ($n = 40$). Then, we compared the volumetric differences and correlations of these subsamples to each other.

3 | RESULTS

3.1 | Volumetric differences between FSL-FIRST pipelines

FSL None produced the highest volumes for the hippocampus, amygdala, caudate and nucleus accumbens and produced the same result as the *FSL Default* pipeline in the other three structures: the putamen, GP and the thalamus. The other pipelines, *FSL Default* and *FSL Fast*, had considerably lower volumes for the hippocampus and amygdala and yielded the exact same result for both structures. *FSL Default* and *FSL Fast* performed very similarly throughout and showed the exact same volumes also for the caudate and the nucleus accumbens. The volumes for each pipeline and structure are presented in Table 2. The identical results in some of the structures are caused by utilising the same boundary correction options.

The volume difference between FSL-FIRST and manual segmentation was highest with the *FSL None* pipeline. The highest volumetric differences were in the amygdala and nucleus accumbens. *FSL Fast* underestimated volumes for the putamen, GP, thalamus and caudate, whereas *FSL Default* underestimated the caudate volume. *FSL None* overestimated the volume for every structure. The percentage differences for each structure and each pipeline are presented in Table 2.

3.2 | FSL-FIRST volumetric correlation analysis

Pearson correlation coefficients between FSL-FIRST and manual segmentation were generally good. Small structures such as the amygdala and nucleus accumbens produced slightly lower values than the rest of the structures. Differences between FSL-FIRST's pipelines were minor. Values for Pearson correlation coefficient for all structures are presented in Table 3. A scatter plot illustration for all structures and methods is provided in Figures 1–8.

ICC (A, k) between FSL-FIRST and manual segmentation were notably lower for *FSL-None* compared with the other pipelines for the hippocampus, amygdala, caudate and nucleus accumbens. For the rest of the structures, the differences between pipelines were generally minor. Intraclass correlation values for each structure and pipeline are presented in Table 3.

3.3 | FreeSurfer volumetric analysis

FreeSurfer produced higher volumes than any of the FSL-FIRST pipelines in the amygdala, putamen and GP. Compared with manual segmentation, FreeSurfer had higher volumes in all structures except for the caudate. Mean volumes and percentage differences for all other structures are presented in Table 2.

3.4 | FreeSurfer volumetric correlation analysis

Pearson correlation coefficients between FreeSurfer and manual segmentation were lower than any of the FSL-FIRST pipelines in all structures except the caudate, where the values were similar. Results were also similar regarding the ICC, where FreeSurfer produced overall lower values compared with FSL-FIRST except for the caudate, where its values were similar compared with *FSL Default* and *FSL Fast* pipelines. Pearson and ICC values for all structures are presented in Table 3.

3.5 | DSC analysis

DSC values between manual segmentation and automated methods were good across the board. FSL-FIRST provided overall slightly higher scores than FreeSurfer for all structures. All automated techniques produced lower results for the amygdala and nucleus accumbens.

TABLE 3 Comparison of correlation analysis between manual and automated segmentation techniques (FSL-FIRST, FreeSurfer)

	FSL-FIRST			FreeSurfer
	Default	Fast	None	
PCC				
L-hippocampus	0.83	0.83	0.86	0.47
R-hippocampus	0.74	0.74	0.75	0.54
L-amygdala	0.61	0.61	0.67	0.34
R-amygdala	0.66	0.66	0.67	0.47
L-thalamus	0.86	0.87	0.86	0.60
R-thalamus	0.89	0.88	0.89	0.61
L-putamen	0.98	0.97	0.98	0.82
R-putamen	0.98	0.96	0.98	0.84
L-GP	0.94	0.89	0.94	0.49
R-GP	0.92	0.87	0.92	0.52
L-caudate	0.78	0.78	0.69	0.84
R-caudate	0.87	0.87	0.80	0.80
L-accumbens	0.69	0.69	0.77	0.44
R-accumbens	0.81	0.81	0.76	0.56
L-cau + acc	0.77	0.77	0.70	0.83
R-cau + acc	0.85	0.85	0.78	0.81
Combined mean	0.83	0.82	0.82	0.60
ICC (A, k)				
L-hippocampus	0.75	0.75	0.34	0.20
R-hippocampus	0.68	0.68	0.28	0.23
L-amygdala	0.55	0.55	0.29	0.09
R-amygdala	0.58	0.58	0.31	0.07
L-thalamus	0.66	0.72	0.66	0.66
R-thalamus	0.69	0.70	0.69	0.66
L-putamen	0.93	0.95	0.93	0.84
R-putamen	0.90	0.92	0.90	0.82
L-GP	0.82	0.53	0.82	0.26
R-GP	0.85	0.46	0.85	0.39
L-caudate	0.85	0.85	0.37	0.90
R-caudate	0.89	0.89	0.53	0.85
L-accumbens	0.69	0.69	0.33	0.58
R-accumbens	0.65	0.65	0.31	0.27
L-cau + acc	0.87	0.87	0.31	0.91
R-cau + acc	0.91	0.91	0.43	0.90
Combined mean	0.75	0.71	0.54	0.49

Notes: Pearson correlation coefficients (PCC) and intraclass correlation coefficients (ICC) (A, k) computed between manual and automatic segmentation volumes. *P*-values for PCC were on all structures $p < 0.001$. Abbreviations: Cau + acc, combined volume of the caudate and nucleus accumbens; Combined mean, mean of all structures combined; GP, globus pallidus; L, left; R, right.

DSC values for all structures and methods are presented in Table 4.

3.6 | Intra-rater data analysis

Volumetric differences between intra-rater segmentations were minor across the board. The largest differences were observed in the hippocampus, amygdala and nucleus accumbens. Correlations were strong across the board. Volumes and volume differences for all structures are presented in Table 5. Correlations and DSC values for all structures are presented in Table 6.

3.7 | Manual segmentations based on FSL-FIRST none and FreeSurfer

The manual segmentation results based on FSL-FIRST None and FreeSurfer were generally in good agreement. The largest volumetric differences were seen in amygdala (FreeSurfer 25.6% larger on the left, 40.7% larger on the right). All other differences were under 15%. Generally manual segmentation based on FreeSurfer produced slightly lower volumes. Mean volumes for both methods are presented in Table 7. Similarly, Pearson correlation coefficients, ICC (A, k) and DSC values were generally good, the lowest values being in bilateral amygdala and nucleus accumbens. The details are presented in Table 8.

3.8 | Analysis of edits that were performed during manual segmentation

The edits were documented on 40 randomly chosen subjects of the total 80 to describe the workflow and also to highlight important areas for quality control. The hippocampus and amygdala consistently required the most edits. The hippocampus had two typical errors that required major manual corrections in most subjects: The lateral anterior superior border was overestimated in 35 and 36 subjects in the left and right hippocampus, respectively, and the inferior posterior area was too large in 30 and 32 subjects in the left and right hippocampus, respectively. The amygdala needed major edits on all subjects. The lateral superior border was overestimated in all subjects, and the anterior side was underestimated in 33 and 35 subjects for the left and right amygdala, respectively. The lateral inferior edge was too large in 21 on the left side and 18 on the right side. The thalami were overall slightly too big and needed minor edits throughout the structure, most notably on the medial posterior

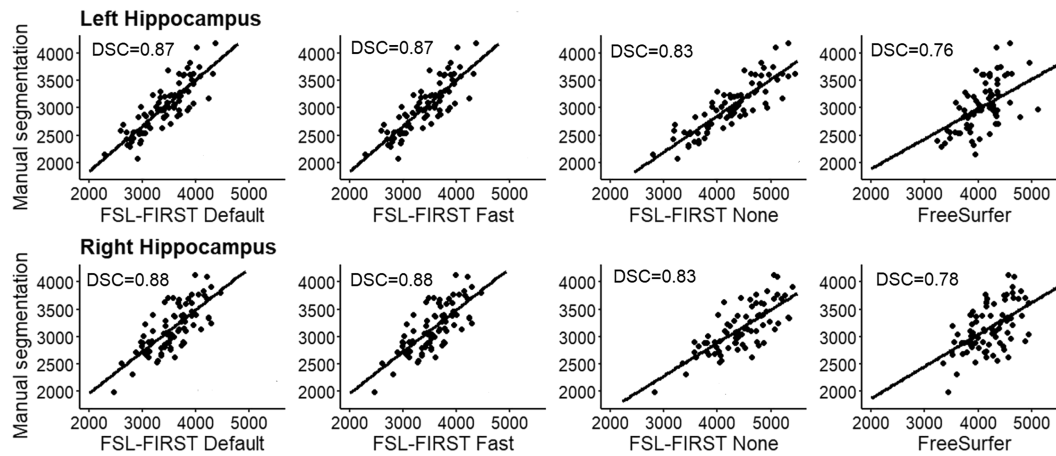


FIGURE 1 Scatter plots of automated segmentation methods against manual segmentation for the hippocampus. DSC, dice score coefficient

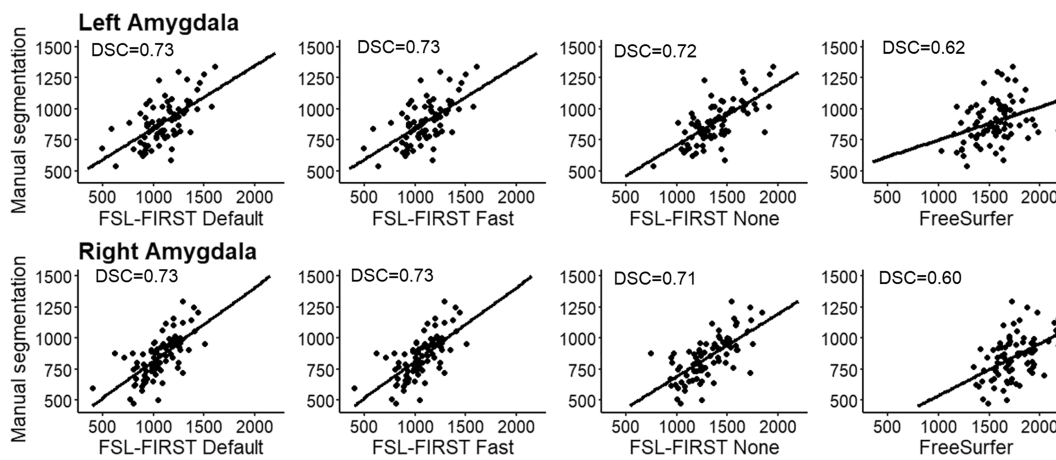


FIGURE 2 Scatter plots of automated segmentation methods against manual segmentation for the amygdala. DSC, dice score coefficient

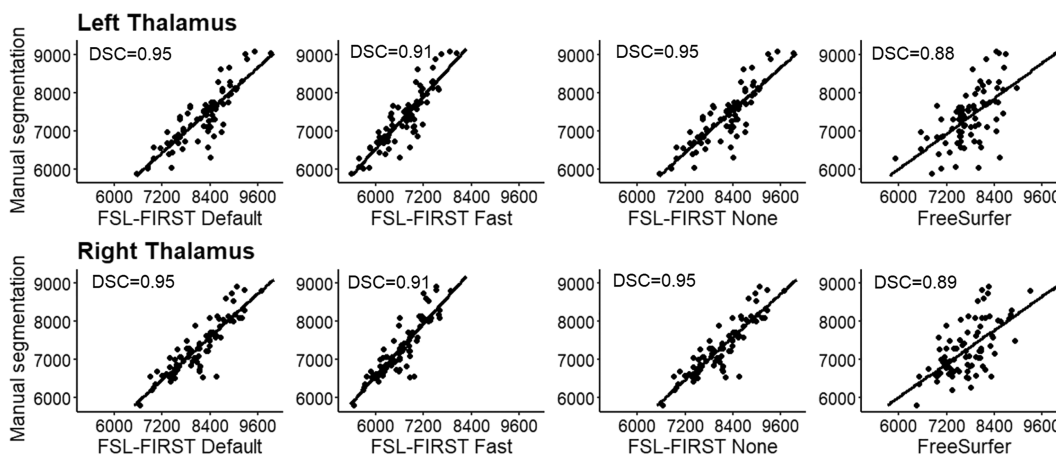


FIGURE 3 Scatter plots of automated segmentation methods against manual segmentation for the thalamus. DSC, dice score coefficient

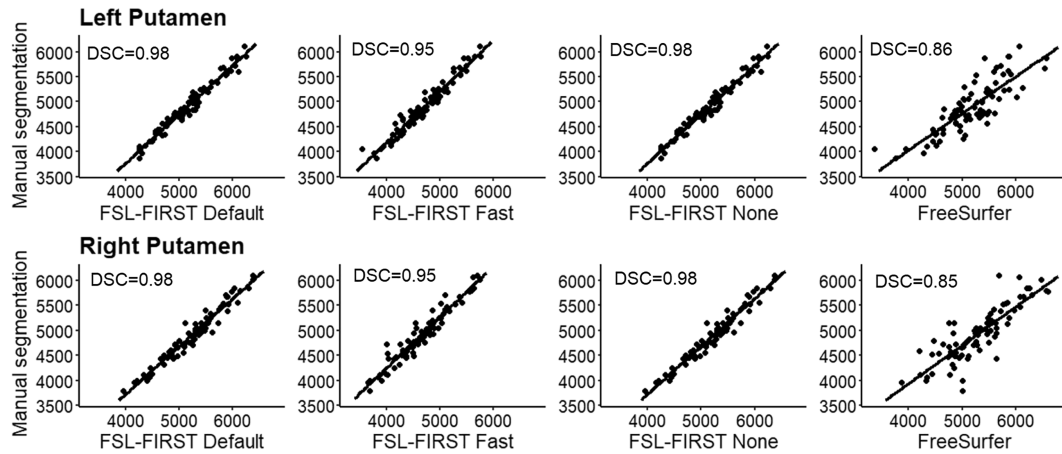


FIGURE 4 Scatter plots of automated segmentation methods against manual segmentation for the putamen. DSC, dice score coefficient

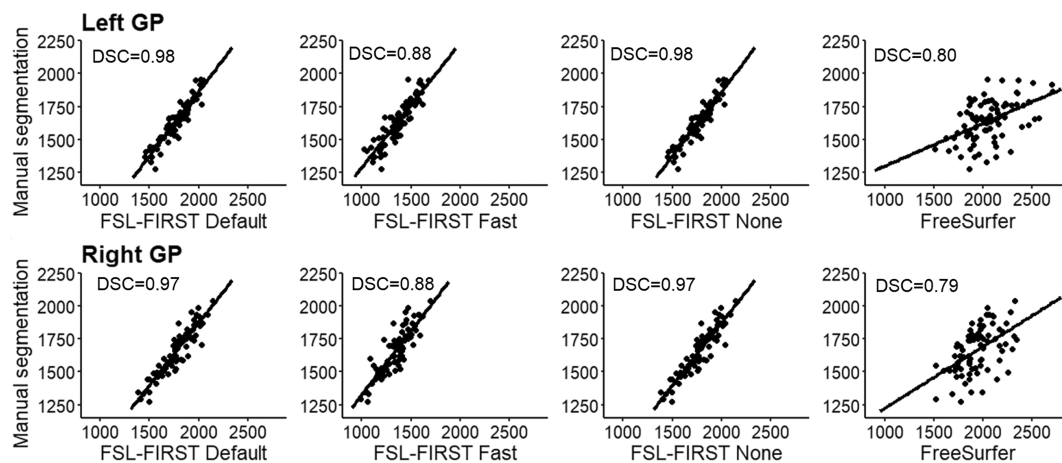


FIGURE 5 Scatter plots of automated segmentation methods against manual segmentation for the GP. DSC = dice score coefficient.

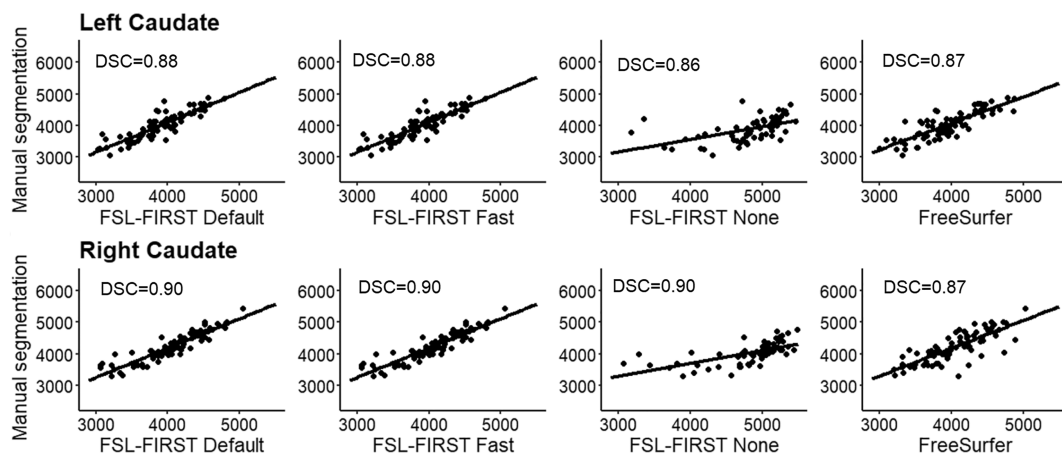


FIGURE 6 Scatter plots of automated segmentation methods against manual segmentation for the caudate. DSC, dice score coefficient

inferior edge, which was overestimated in 21 subjects for the left and in 19 for the right thalamus. The caudate received most edits on the lateral posterior inferior area,

where the *FSL None* pipeline overestimated the border in 30 subjects for the left and in 26 for the right caudate. Notably, the superior medial area of the right caudate

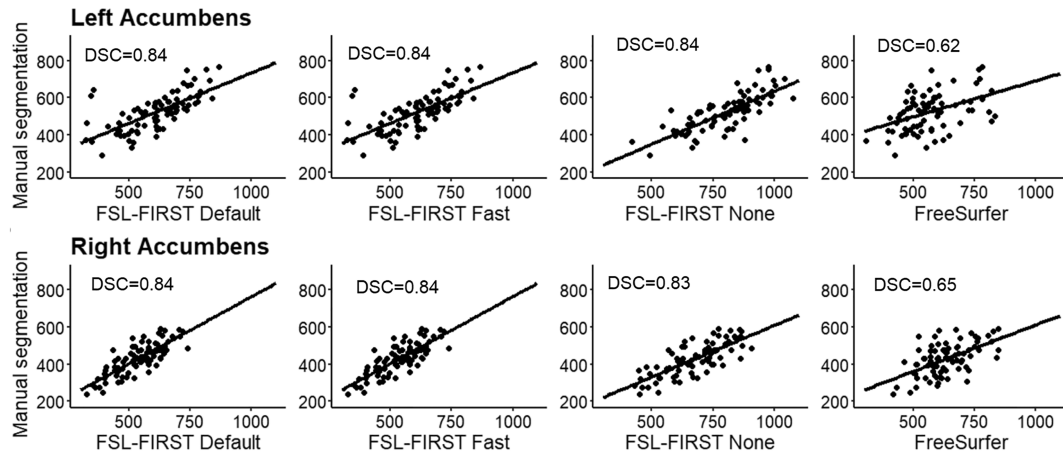


FIGURE 7 Scatter plots of automated segmentation methods against manual segmentation for the nucleus accumbens. DSC, dice score coefficient

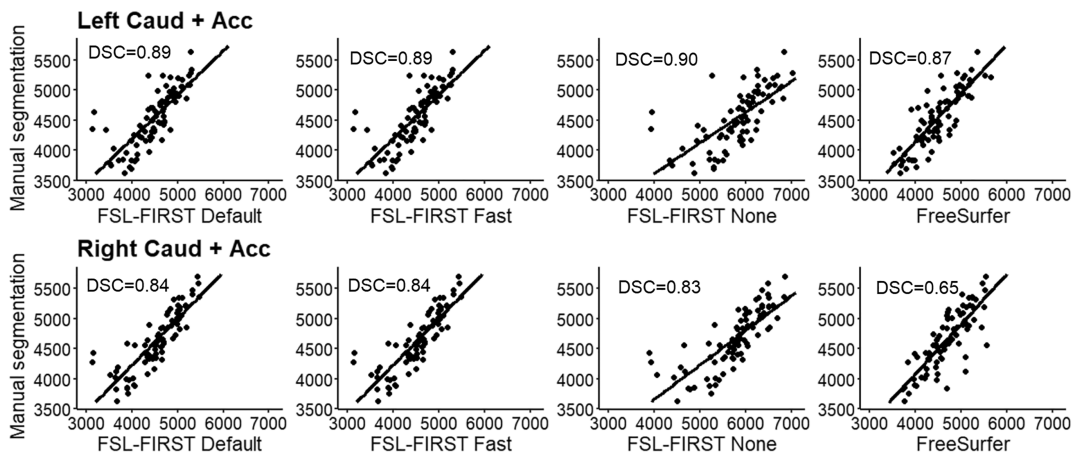


FIGURE 8 Scatter plots of automated segmentation methods against manual segmentation for the combined segmentations of caudate and nucleus accumbens. DSC, dice score coefficient

was too large in 17 subjects, whereas on the left it was only overestimated in three subjects. All common edits are listed in Table 9. The putamen, GP and nucleus accumbens were more accurately segmented by FSL-FIRST than by FreeSurfer and only received minor and sporadic edits.

3.9 | Split-half analysis

The volumetric differences in the split-half analysis were small between the halves. The volumetric differences between the halves ranged from 0 percentage points to 5 percentage points, with most structures the difference was between 1 and 2 percentage points. The correlation value differences between halves were generally slightly larger than the volumetric differences. Most of the

structures yielded similar correlations for both halves; FreeSurfer produced slightly larger differences in correlations compared with FSL-FIRST's pipelines. Detailed results of the split-half analysis are presented in the Supporting Information.

4 | DISCUSSION

In this study, we compared two automated segmentation tools, FSL-FIRST and FreeSurfer, against manual segmentation on subcortical areas in a paediatric population. We included in the comparisons, FSL-FIRST's three different pipelines—*FSL Default*, *FSL Fast* and *FSL None*—each of which uses different boundary correction settings to determine the exact anatomical borders of structures. Our goal was to compare the accuracy of these automated

TABLE 4 Comparison of mean dice score coefficient values between manual and automated segmentation techniques

	FSL-FIRST			FreeSurfer
	Default	Fast	None	
DSC (SD)				
L-hippocampus	0.87 (0.03)	0.87 (0.03)	0.83 (0.04)	0.76 (0.05)
R-hippocampus	0.88 (0.03)	0.88 (0.03)	0.83 (0.04)	0.78 (0.04)
L-amygdala	0.73 (0.05)	0.73 (0.05)	0.72 (0.05)	0.62 (0.07)
R-amygdala	0.73 (0.06)	0.73 (0.06)	0.71 (0.06)	0.60 (0.07)
L-thalamus	0.95 (0.02)	0.91 (0.01)	0.95 (0.02)	0.88 (0.02)
R-thalamus	0.95 (0.02)	0.91 (0.01)	0.95 (0.02)	0.89 (0.02)
L-putamen	0.98 (0.01)	0.95 (0.01)	0.98 (0.01)	0.86 (0.02)
R-putamen	0.98 (0.01)	0.95 (0.01)	0.98 (0.01)	0.85 (0.03)
L-GP	0.98 (0.01)	0.88 (0.03)	0.98 (0.01)	0.80 (0.05)
R-GP	0.97 (0.02)	0.87 (0.03)	0.97 (0.02)	0.79 (0.06)
L-caudate	0.88 (0.04)	0.88 (0.04)	0.86 (0.05)	0.87 (0.03)
R-caudate	0.90 (0.03)	0.89 (0.03)	0.90 (0.04)	0.87 (0.02)
L-accumbens	0.84 (0.05)	0.84 (0.05)	0.84 (0.05)	0.62 (0.07)
R-accumbens	0.84 (0.03)	0.84 (0.03)	0.83 (0.04)	0.65 (0.06)
L-cau + acc	0.89 (0.03)	0.89 (0.03)	0.90 (0.04)	0.87 (0.02)
R-cau + acc	0.84 (0.03)	0.84 (0.03)	0.83 (0.04)	0.65 (0.06)
Combined mean	0.89	0.87	0.88	0.77

Note: Comparison of Dice score coefficient (DSC) mean values between manual and automated segmentation techniques.

Abbreviations: Cau + acc, score calculated with the combined area of the caudate and the nucleus accumbens; Combined mean, mean score of all structures; GP, globus pallidus; L, left; R, right; SD, standard deviation.

segmentation methods with manual segmentation, which is currently considered the gold standard (Hashempour et al., 2019; Morey et al., 2009) and has been validated as such in previous articles in paediatric as well as adult populations (Makowski et al., 2018; Schoemaker et al., 2016). In our results, *FSL Default* and *FSL Fast* pipelines performed overall more accurately than *FSL None* or FreeSurfer. We observed that automated methods tend to overestimate volumes in most structures, as was expected based on previous studies (Grimm et al., 2015; Hashempour et al., 2019; Nugent et al., 2013; Pipitone et al., 2014). The overestimation was overall most prominent with FreeSurfer and *FSL None*, although there were some notable exceptions in specific structures, such as the caudate, where FreeSurfer slightly underestimated volumes. Excluding the *FSL None* pipeline, FSL-FIRST produced generally better agreement across the structures than FreeSurfer.

4.1 | Hippocampus and amygdala

Both hippocampus and amygdala were overestimated by all automated segmentation methods in our study. Most

accurate were *FSL Default* and *FSL Fast* pipelines with a moderate overestimation. *FSL None* and FreeSurfer overestimated both structures greatly. With all methods, the overestimation was more prominent in the amygdala than the hippocampus, which has also been documented in previous articles in adults as well as paediatric populations (Akudjedu et al., 2018; Doring et al., 2011; Pipitone et al., 2014; Schoemaker et al., 2016).

FSL Default and *FSL Fast* had overall better correlations with manual segmentation than *FSL None* or FreeSurfer. For the hippocampus, all of FSL-FIRST's pipelines exceeded the threshold coefficient of $r > 0.70$, which has previously been suggested as the minimum for defining reliability between measures (Terwee et al., 2007). The Pearson correlation coefficients for the amygdala were lower, ranging from $r = 0.61$ to $r = 0.67$ with FSL-FIRST's pipelines. FreeSurfer's correlations were significantly weaker than FSL-FIRST's for both hippocampus and amygdala, with amygdala having the lowest values. *FSL Default* and *FSL Fast* produced identical intraclass correlation (A, k) values, whereas *FSL None* and FreeSurfer showed very low to no correlation, indicating a large estimation bias. Automated segmentation of the hippocampus tends to have better consistency and

TABLE 5 Comparison of mean (standard deviation) volumes and percentage of volume difference in intra-rater segmentations

	1st segmentation	Re-segmentation	Paired samples <i>t</i> -test (<i>p</i> -value)
Volume (SD)			
L-hippocampus	2890.1 (379.19)	2798.1 (306.03)	1.79 (0.10)
R-hippocampus	3106.2 (400.16)	2911.4 (218.02)	2.18 (0.06)
L-amygdala	868.8 (195.77)	851.9 (110.08)	0.42 (0.69)
R-amygdala	846.1 (205.69)	861.3 (132.26)	-0.49 (0.63)
L-thalamus	7545.5 (886.07)	7569.2 (737.32)	-0.12 (0.90)
R-thalamus	7532.2 (878.53)	7629.0 (698.94)	-0.56 (0.59)
L-putamen	5241.7 (533.12)	5198.0 (519.37)	0.98 (0.35)
R-putamen	5131.8 (660.93)	5119.1 (622.32)	0.30 (0.77)
L-GP	1726.2 (167.95)	1725.6 (177.97)	0.05 (0.96)
R-GP	1709.9 (173.41)	1713.97 (179.18)	-0.01 (0.92)
L-caudate	3951.6 (439.06)	4030.8 (438.48)	1.49 (0.17)
R-caudate	4146.2 (483.86)	4268.3 (508.84)	-2.01 (0.07)
L-accumbens	522.4 (100,92)	553.7 (70,17)	-1.49 (0.17)
R-accumbens	446.8 (108,12)	472.1 (107,57)	-2.01 (0.07)
L-cau + acc	4474.0 (486.24)	4584.5 (477.37)	-1.61 (0.14)
R-cau + acc	4593.0 (526.08)	4740.4 (552.61)	-2.10 (0.06)
Combined mean	3420.78	3439.21	
% volume diff. (SD)			
L-hippocampus		-2.81 (5.27)	
R-hippocampus		-5.46 (8.33)	
L-amygdala		0.48 (13.94)	
R-amygdala		4.35 (12.76)	
L-thalamus		0.82 (8.19)	
R-thalamus		1.82 (7.94)	
L-putamen		-0.79 (2.62)	
R-putamen		-0.14 (2.67)	
L-GP		-0.06 (2.48)	
R-GP		0.34 (6.29)	
L-caudate		2.12 (4.51)	
R-caudate		3.03 (4.65)	
L-accumbens		8.33 (18,63)	
R-accumbens		6.40 (10,41)	
L-cau + acc		2.64 (5.13)	
R-cau + acc		3.31 (4.74)	
Combined mean		1.52	

Notes: The volumetric unit used is 1 voxel (= 1 mm³). Description of mean volumes and mean percentage of volume difference (% volume diff.) in intra-rater segmentations.

Abbreviations: Cau + acc, combined volume of the caudate and nucleus accumbens;

Combined mean, mean of all structures combined; GP, globus pallidus; L, left; R, right; SD, standard deviation.

reproducibility than the amygdala, which has been shown in multiple previous studies (Morey et al., 2009; Nugent et al., 2013; Pardoe et al., 2009; Schoemaker

et al., 2016) that reported Pearson correlation coefficients ranging from $r = 0.47$ to $r = 0.67$ for the hippocampus and $r = 0.24$ to $r = 0.35$ for the amygdala

TABLE 6 Comparison of correlation analysis between intra-rater data

	PCC	ICC (A, k)	DSC (SD)
L-hippocampus	0.91	0.93	0.91 (0.03)
R-hippocampus	0.73	0.70	0.90 (0.03)
L-amygdala	0.80	0.82	0.82 (0.11)
R-amygdala	0.92	0.92	0.86 (0.06)
L-thalamus	0.76	0.87	0.96 (0.03)
R-thalamus	0.78	0.87	0.96 (0.02)
L-putamen	0.96	0.98	0.98 (0.01)
R-putamen	0.98	0.99	0.98 (0.01)
L-GP	0.97	0.99	0.98 (0.01)
R-GP	0.81	0.91	0.97 (0.02)
L-caudate	0.93	0.96	0.94 (0.02)
R-caudate	0.93	0.95	0.95 (0.02)
L-accumbens	0.63	0.73	0.90 (0.06)
R-accumbens	0.91	0.94	0.91 (0.03)
L-cau + acc	0.90	0.94	0.94 (0.02)
R-cau + acc	0.92	0.94	0.95 (0.02)
Combined mean	0.87	0.90	0.93

Notes: Pearson correlation coefficients (PCC), intraclass correlation coefficients (ICC) (A, k) and mean dice score correlation coefficient (DSC) computed between intra-rater volumes. PCC p -values were $p < 0.05$ for all structures.

Abbreviations: Cau + acc, combined volume of the caudate and nucleus accumbens; Combined mean, mean of all structures combined; GP, globus pallidus; L, left; R, right; SD, standard deviation.

using FSL-FIRST and $r = 0.67$ to $r = 0.82$ and $r = 0.45$ to $r = 0.61$ for the hippocampus and amygdala, respectively, using FreeSurfer. Similar results were shown regarding the DSC with every automated method producing higher mean values for the hippocampus (DSC > 0.76) than the amygdala (DSC > 0.60) in our results. The studies conducted by Morey et al. and Pardoe et al. also included DSC analysis showing results of the hippocampus producing higher spatial overlap than the amygdala with both FSL-FIRST and FreeSurfer, which is in line with our findings.

We found that FreeSurfer performed poorer than FSL-FIRST overall. This was an unexpected finding, as FreeSurfer has previously been reported to be overall more accurate and consistent than FSL-FIRST for both the hippocampus and amygdala for paediatric and adult populations (Morey et al., 2009; Schoemaker et al., 2016). Inter-rater variability may have contributed to these differences, as it is one of the key challenges with manual segmentation. The differences can be more pronounced in structures such as the amygdala, where the border around the structure may be difficult to distinguish

visually. In these instances, the rater must rely on general anatomical knowledge instead of the intensities of the MR image to determine the exact shape of the structure. This is even more significant in paediatric MR images, because they have different contrast and comparatively lower resolution than adult images (Gousias et al., 2012). Example segmentations of the hippocampus and amygdala are presented in Figure 9.

4.2 | Thalamus

The thalamus was most accurately segmented by FreeSurfer with only a slight overestimation. *FSL Default* and *FSL None* pipelines produced a larger overestimation, whereas *Fast* underestimated the volume. Previous studies have shown results of FreeSurfer producing larger or similar volumes compared to FSL-FIRST (Hannoun et al., 2019; Makowski et al., 2018; Næss-Schmidt et al., 2016). The discrepancy in results might be partly caused by inter-rater variability between the researchers in different studies. Despite having the most accurate mean volume, FreeSurfer's Pearson correlation coefficient was significantly worse, $r = 0.60$, than any of FSL-FIRST's pipelines, ranging from $r = 0.86$ to $r = 0.89$, indicating a larger volumetric variation in individual segmentations. Intraclass correlation (A, k) was on similar levels with coefficients ranging from ICC = 0.66 to ICC = 0.72, with all methods, suggesting a low to moderate reproducibility rate with manual segmentation. One previous study (Makowski et al., 2018) also showed weaker Pearson correlations for both FreeSurfer and FSL-FIRST than our results, ranging from $r = 0.37$ to $r = 0.44$, but included a significantly smaller sample size of 30 adults and that may explain some of the differences. The DSC values were great for all methods in our study, DSC > 0.91 for FSL-FIRST and DSC > 0.88 for FreeSurfer. A previous study done by Hannoun et al. (2019), including subjects aged between 1 and 18 years, showed similar results with DSC = 0.86 for FSL-FIRST and DSC = 0.84 for FreeSurfer. Segmentations of the thalamus are presented in Figures 10 and 11.

4.3 | Putamen and GB

The putamen was segmented more accurately than the GP by all methods in this study. *FSL Default* and *FSL None* as well as FreeSurfer overestimated the putamen slightly, whereas *Fast* produced an underestimation of a similar volume. Similar results were observed with the GP, but with a greater magnitude. A previous study yielded similar results with FreeSurfer producing a

TABLE 7 Volumetric comparison of manual segmentations based on FSL-FIRST none and FreeSurfer automated segmentations

	Manual segmentation (FIRST)	Manual segmentation (FreeSurfer)
Volume (SD)		
L-hippocampus	2999.95 (486.84)	2784.80 (242.51)
R-hippocampus	3215.05 (511.68)	2907.05 (309.86)
L-amygdala	916.15 (196.17)	1112.95 (152.08)
R-amygdala	873.75 (207.16)	1181.05 (152.78)
L-thalamus	7380.75 (861.55)	6797.00 (605.05)
R-thalamus	7311.45 (800.43)	6707.80 (619.48)
L-putamen	5006.70 (579.70)	4894.85 (516.16)
R-putamen	4990.00 (589.59)	4833.95 (546.43)
L-GP	1674.70 (150.39)	1645.05 (246.21)
R-GP	1690.05 (181.08)	1499.65 (164.35)
L-caudate	3999.00 (519.02)	3636.2 (542.85)
R-caudate	4216.80 (539.52)	3696.25 (533.02)
L-accumbens	520.90 (102.06)	438.00 (98.98)
R-accumbens	429.20 (88.14)	462.90 (100.68)
L-cau + acc	4519.90 (567.87)	4074.20 (604.42)
R-cau + acc	4646.00 (566.61)	4159.15 (596.60)
Combined mean	3399.40	3176.93
% volume diff. (SD)		
L-hippocampus		-5.39 (13.81)
R-hippocampus		-8.35 (10.40)
L-amygdala		25.63 (26.91)
R-amygdala		40.73 (28.44)
L-thalamus		-7.86 (8.59)
R-thalamus		-7.86 (7.27)
L-putamen		-1.95 (6.13)
R-putamen		-2.79 (7.23)
L-GP		-1.76 (11.52)
R-GP		-10.86 (8.56)
L-caudate		-9.07 (6.69)
R-caudate		-12.47 (3.95)
L-accumbens		-13.37 (24.10)
R-accumbens		10.40 (26.05)
L-cau + acc		-9.34 (7.25)
R-cau + acc		-10.62 (4.71)
Combined mean		-1.56

Notes: The volumetric unit used is 1 voxel (= 1 mm³). Description of mean volumes obtained from manual segmentations based on FSL-FIRST and FreeSurfer as well as mean percentage of volume difference (% volume diff.) between FSL-FIRST and FreeSurfer based manual segmentation.

Abbreviations: Cau + acc, combined volume of the caudate and nucleus accumbens; Combined mean, mean of all structures combined; GP, globus pallidus; L, left; R, right; SD, standard deviation.

higher overestimations than FIRST and GP having a greater relative volume difference than the putamen (Velasco-Annis et al., 2017). FSL-FIRST had excellent

correlations for both putamen and GP, ranging from $r = 0.86$ to $r = 0.98$ across all pipelines. FreeSurfer also had a strong correlation for the putamen but performed

TABLE 8 Comparison of correlation analysis between manual segmentation based on FSL-FIRST none and FreeSurfer

	PCC	ICC (A, k)	DSC
L-hippocampus	0.63	0.62	0.85 (0.03)
R-hippocampus	0.75	0.70	0.86 (0.03)
L-amygdala	0.36	0.36	0.76 (0.05)
R-amygdala	0.64	0.41	0.76 (0.07)
L-thalamus	0.65	0.64	0.91 (0.02)
R-thalamus	0.72	0.68	0.92 (0.02)
L-putamen	0.84	0.91	0.91 (0.01)
R-putamen	0.79	0.87	0.91 (0.02)
L-GP	0.62	0.72	0.86 (0.03)
R-GP	0.65	0.58	0.83 (0.04)
L-caudate	0.87	0.83	0.90 (0.03)
R-caudate	0.96	0.79	0.90 (0.02)
L-accumbens	0.17	0.23	0.72 (0.08)
R-accumbens	0.47	0.62	0.75 (0.07)
L-cau + acc	0.83	0.79	0.90 (0.03)
R-cau + acc	0.94	0.82	0.90 (0.02)
Combined mean	0.68	0.66	0.85

Notes: Pearson correlation coefficients (PCC), intraclass correlation coefficients (ICC) (A, k) and mean Dice score coefficients (DSC) computed between manual segmentations based on FSL-FIRST and FreeSurfer. *P* values for PCC were $p < 0.01$ for all structures.

Abbreviations: Cau + acc, combined volume of the caudate and nucleus accumbens; Combined mean, mean of all structures combined; GP, globus pallidus; L, left; R, right; SD, standard deviation.

significantly weaker for the GP with coefficients of $r = 0.49$ and $r = 0.52$ for the left and right GP. ICC (A, k) were high across the board, with all methods yielding a coefficient of ICC > 0.80 for the putamen. For the GP, intraclass correlations were significantly lower for *FSL Fast* and FreeSurfer, whereas *FSL Default* and *FSL None* had great values of ICC > 0.80 for both structures, indicating a small estimation bias and good reproducibility with manual segmentation. A 2017 published study showed FreeSurfer having slightly better segmentation reproducibility for both the putamen and GP (Velasco-Annis et al., 2017). Another study published in 2018 showed the opposite and indicated that for FSL-FIRST has better consistency for the GP segmentation (Makowski et al., 2018). Direct comparison of these results is not ideal because both studies were done on an adult population and included a sample size of 30 or less. The DSC results in our study were great across the board with FSL-FIRST producing excellent results of DSC > 0.90 for both the putamen and GP with all techniques. FreeSurfer's results were lower, but still satisfactory, DSC > 0.79 . A previous study showed similar

TABLE 9 Most common major edits to structures and areas using the *FSL-none* segmentations out of 40 randomly chosen images

Edited areas	Number of subjects edited	
	Left	Right
Hippocampus		
Lateral anterior superior area overestimated	35	36
Inferior posterior area overestimated	30	32
Uneven anterior end	12	13
Amygdala		
Lateral superior posterior area overestimated	39	40
Anterior side underestimated	33	35
Lateral inferior edge overestimated	21	18
Thalamus		
Medial posterior inferior edge overestimated	21	19
Anterior end overestimated	5	5
Posterior inferior edge overestimated	3	2
Caudate		
Lateral posterior inferior area overestimated	30	26
Superior medial area overestimated	3	17
Superior medial anterior edge underestimated	8	7
Superior medial inferior edge underestimated	5	2

results with FSL-FIRST (DSC > 0.90), producing slightly higher DSC values than FreeSurfer (DSC > 0.80) for the putamen (Perlaki et al., 2017). However, the age of the subjects was not specified, so the results may not be adequately comparable with our findings. To our knowledge, this is the first automated segmentation method validation study done on a paediatric population including the putamen and GP. Segmentations of the putamen and GP are presented in Figure 10.

4.4 | Caudate and nucleus accumbens

The caudate was overall segmented accurately, whereas the nucleus accumbens was overestimated by all methods in our study. The caudate was segmented accurately by all methods excluding *FSL None*, which overestimated both the caudate and the nucleus accumbens significantly. FreeSurfer and FSL-FIRST's other pipelines produced an accurate volume for the caudate with only a minor underestimation. The nucleus accumbens was

FIGURE 9 Transversal view of the segmentations of the hippocampus and amygdala. Yellow, hippocampus; turquoise, amygdala

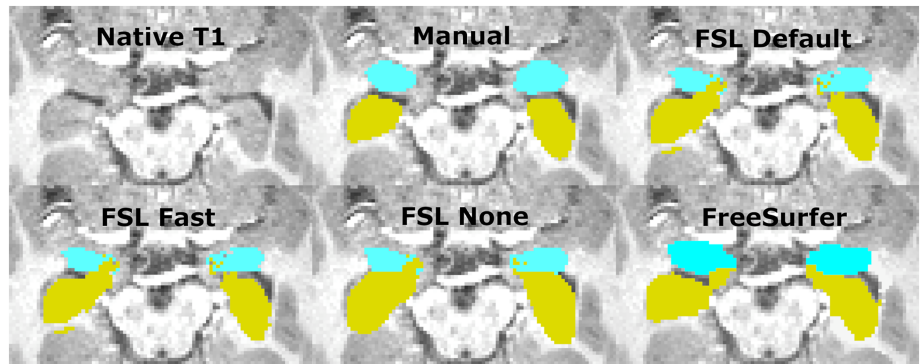
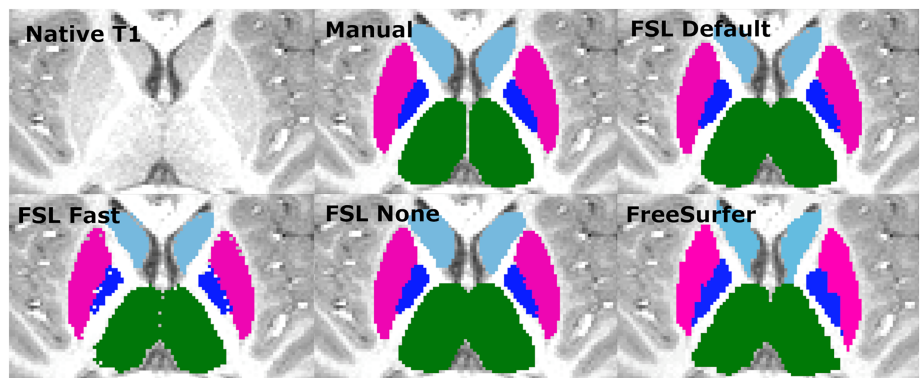


FIGURE 10 Transversal view of segmentations of the putamen, globus pallidus (GP), thalamus and caudate. Putamen, pink; GP, blue; thalamus, green; caudate, light blue



overestimated by all methods, with *FSL None* and FreeSurfer yielding the highest volumes. Notable is also the more prominent overestimation of the right nucleus accumbens, compared with the left, which was present in all four automated methods. Previous research indicates a moderate overestimation of both the caudate and nucleus accumbens with both FSL-FIRST and FreeSurfer (Perlaki et al., 2017; Velasco-Annis et al., 2017) with similar volumetric values compared with our results.

Pearson correlations coefficients were strong across all methods for the caudate, ranging from $r = 0.69$ to $r = 0.84$, showing a strong relationship between manual segmentation and the automated methods. The nucleus accumbens has similar coefficient values regarding FSL-FIRST, but FreeSurfer produced significantly weaker correlations. The ICC (A, k) showed that *FSL Default* and *FSL Fast* had superior reproducibility compared with *FSL None* and FreeSurfer for the nucleus accumbens. The results are similar for the caudate with the exception of FreeSurfer performing just as good as *FSL Default* and *FSL Fast*, with ICC values ranging from $ICC = 0.85$ to $ICC = 0.90$, whereas *FSL None's* coefficients were significantly lower at $ICC = 0.37$ and $ICC = 0.53$ for the left and right caudate, respectively. The consistency and reproducibility of the caudate and nucleus accumbens have been documented in previous

studies with slightly different results compared with our study (Perlaki et al., 2017; Velasco-Annis et al., 2017). The article by Velasco-Annis et al. suggested great reproducibility rates for the caudate with both FreeSurfer and FSL-FIRST, with ICC values ranging from $ICC = 0.86$ to $ICC = 0.93$, producing similar values for each method. The other study conducted by Perlaki et al. showed a slightly better reproducibility with FreeSurfer regarding the caudate and nucleus accumbens. The study by Perlaki et al. (2017) also showed results similar to ours regarding the DSC values with FSL-FIRST producing better slightly better values than FreeSurfer for the caudate.

Overall, these variations in results may be explained with the difficult determination of the border between the caudate and nucleus accumbens. The intensities of the MR image are visually indistinguishable for these two structures, which may lead to inaccuracy in volumetric quantification. To assess this problem, we combined the volumes of both structures to eliminate possible errors caused by the similarity of intensities. Considering the relatively small volume of the nucleus accumbens, the results for combined volume were similar to the results derived from the caudate volumes. Segmentations of the caudate and nucleus accumbens are presented in Figure 11.

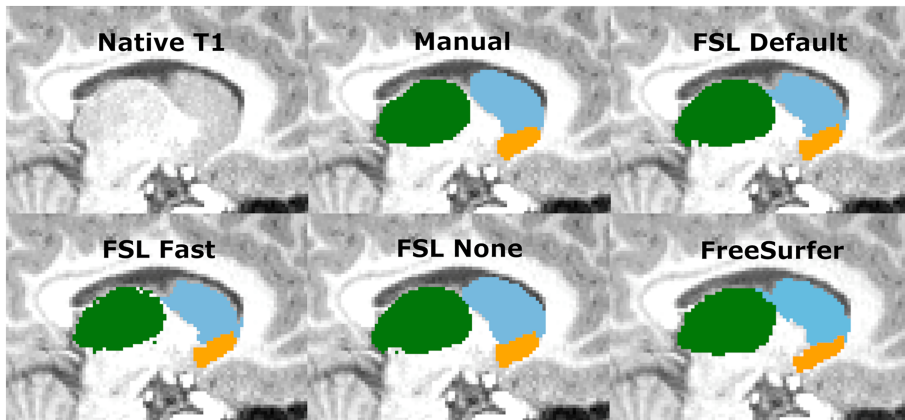


FIGURE 11 Sagittal view of the thalamus, caudate and nucleus accumbens. Thalamus, green; caudate, light blue; nucleus accumbens, orange

4.5 | Limitations

Our study presents a few limitations. Firstly, the sample size is limited due to the time-consuming manual segmentation process but likely sufficient for building study-specific templates, which is a potential goal for applied studies (Lee et al., 2019). Secondly, all manual segmentations were performed by a single rater, which might lead to some systematic biases in delineation of anatomical borders in MR images. However, the expert review provides some safeguard for this. On a related note, the manual segmentation was done by editing models produced by *FSL None*, which might potentially cause the manual segmentations to have a bias towards FSL-FIRST. However, this was explored by segmenting a subsample based on FreeSurfer automated segmentation. Generally, the results were similar. There were some differences in structures that are smaller and harder to delineate, such as the amygdala and the nucleus accumbens. Additionally, some minor differences are to be expected simply to technical challenges when performing the manual segmentation using two different editing tools. Most importantly, automated FreeSurfer segmentation vastly overestimated amygdala volumes even when compared with the manual segmentation based on it. Therefore, using FreeSurfer segmentation as the basis would not have changed the conclusion that visual inspection for certain structures is strongly advised.

5 | CONCLUSIONS

In this feasibility study, we determined the accuracy of two automated segmentation tools for T1-weighted MR images, FSL-FIRST with three different boundary correction settings and FreeSurfer against manual segmentation in a paediatric 5-year-old population ($N = 80$). Overall, the automated tools show promising accuracies, but the performance of all automated tools changed

vastly based on the structure. Small structures such as the amygdala and nucleus accumbens were inaccurately segmented by all automated methods. On the other hand, the segmentation of the putamen and the caudate were performed accurately with most of the automated methods and yielded relatively good consistency and reproducibility with manual segmentation. The use of these automated segmentation tools in neuroimaging studies still presents challenges, and careful visual inspection of the automated segmentations is still strongly advised, because there are many factors such as the quality of the used MR images that might impact the accuracy of the segmentations. Future research should investigate the benefits of using custom subcortical atlases to improve the accuracy and reliability of automated segmentation methods especially for the amygdala and hippocampus (Lee et al., 2019).

ACKNOWLEDGEMENTS

EPP was supported by the Päivikki and Sakari Sohlberg Foundation. ESI was supported by Juho Vainio Foundation, Finnish Brain Foundation, Turunmaan Duodecim-seura. VK was supported by Finnish Cultural Foundation and Lastenlinnan säätiö. NH was supported by the Orion Research Foundation, the University of Turku Graduate School and the Hospital District of Southwest Finland State Research Grants. LK was supported by Brain and Behavior Research Foundation, National Alliance for Research on Schizophrenia and Depression (NARSAD) (YI Grant No. 1956), State Grants for Clinical Research (ERVA) and the Academy of Finland (Profi 5, No. 325292). SN was supported by the State Grants for Clinical Research. JJT was supported by the Hospital District of Southwest Finland, Turku University Foundation, State Grants for Clinical Research and Emil Aaltonen Foundation and Alfred Kordelin Foundation (data collection and data analysis) as well as Sigrid Jusélius Foundation (interpretation of the data and writing the manuscript).

CONFLICT OF INTEREST

The authors declare no conflict of interest.

PEER REVIEW

The peer review history for this article is available at <https://publons.com/publon/10.1111/ejn.15761>.

DATA AVAILABILITY STATEMENT

Research data are not shared. The ethics committee decision and local legislation do not allow the open sharing of neuroimaging data.

ORCID

Kristian Lidauer  <https://orcid.org/0000-0003-1389-2637>

Elmo P. Pulli  <https://orcid.org/0000-0003-3871-8563>

Anni Copeland  <https://orcid.org/0000-0002-6482-9008>

Eero Silver  <https://orcid.org/0000-0002-9522-7720>

Harri Merisaari  <https://orcid.org/0000-0002-8515-5399>

REFERENCES

- Acosta, H., Kantojärvi, K., Hashempour, N., Pelto, J., Scheinin, N. M., Lehtola, S. J., Lewis, J. D., Fonov, V. S., Collins, D. L., Evans, A., Parkkola, R., Lähdesmäki, T., Saunavaara, J., Karlsson, L., Merisaari, H., Paunio, T., Karlsson, H., & Tuulari, J. J. (2020). Partial support for an interaction between a polygenic risk score for major depressive disorder and prenatal maternal depressive symptoms on infant right amygdalar volumes. *Cerebral Cortex*, *30*, 6121–6134. <https://doi.org/10.1093/cercor/bhaa158>
- Akudjedu, T. N., Nabulsi, L., Makelyte, M., Scanlon, C., Hehir, S., Casey, H., Ambati, S., Kenney, J., O'Donoghue, S., McDermott, E., Kilmartin, L., Dockery, P., McDonald, C., Hallahan, B., & Cannon, D. M. (2018). A comparative study of segmentation techniques for the quantification of brain subcortical volume. *Brain Imaging and Behavior*, *12*(6), 1678–1695. <https://doi.org/10.1007/s11682-018-9835-y>
- Barch, D. M., Harms, M. P., Tillman, R., Hawkey, E., & Luby, J. L. (2019). Early childhood depression, emotion regulation, episodic memory, and hippocampal development. *Journal of Abnormal Psychology*, *128*(1), 81–95. <https://doi.org/10.1037/abn0000392>
- Barch, D. M., Tillman, R., Kelly, D., Whalen, D., Gilbert, K., & Luby, J. L. (2019). Hippocampal volume and depression among young children. *Psychiatry Research: Neuroimaging*, *288*, 21–28. <https://doi.org/10.1016/j.psychresns.2019.04.012>
- Braak, H., & Braak, E. (1991). Neuropathological stageing of Alzheimer-related changes. *Acta Neuropathologica*, *82*, 239–259. <https://doi.org/10.1007/BF00308809>
- Cherbuin, N., Anstey, K. J., Réglade-Meslin, C., & Sachdev, P. S. (2009). In vivo hippocampal measurement and memory: A comparison of manual tracing and automated segmentation in a large community-based sample. *PLoS ONE*, *4*(4), e5265. <https://doi.org/10.1371/journal.pone.0005265>
- Copeland, A., Silver, E., Korja, R., Lehtola, S. J., Merisaari, H., Saukko, E., Sinisalo, S., Saunavaara, J., Lähdesmäki, T., Parkkola, R., Nolvi, S., Karlsson, L., Karlsson, H., & Tuulari, J. J. (2021). Infant and child MRI: A review of scanning procedures. *Frontiers in Neuroscience*, *15*, 666020. <https://doi.org/10.3389/fnins.2021.666020>
- de Macedo Rodrigues, K., Ben-Avi, E., Sliva, D. D., Choe, M., Drottar, M., Wang, R., Fischl, B., Grant, P. E., & Zöllei, L. (2015). A FreeSurfer-compliant consistent manual segmentation of infant brains spanning the 0–2 year age range. *Frontiers in Human Neuroscience*, *9*, 21. <https://doi.org/10.3389/fnhum.2015.00021>
- Doring, T. M., Kubo, T. T. A., Cruz, L. C. H. Jr., Juruena, M. F., Fainberg, J., Domingues, R. C., & Gasparetto, E. L. (2011). Evaluation of hippocampal volume based on MR imaging in patients with bipolar affective disorder applying manual and automatic segmentation techniques. *Journal of Magnetic Resonance Imaging*, *33*(3), 565–572. <https://doi.org/10.1002/jmri.22473>
- Ferri, J., Eisendrath, S. J., Fryer, S. L., Gillung, E., Roach, B. J., Mathalon, D. H., & Francisco, S. (2018). Blunted amygdala activity is associated with depression severity in treatment-resistant depression. *Cognitive, Affective, & Behavioral Neuroscience*, *17*(6), 1221–1231. <https://doi.org/10.3758/s13415-017-0544-6>
- Fischl, B., Salat, D. H., Busa, E., Albert, M., Dieterich, M., Haselgrove, C., Van Der Kouwe, A., Killiany, R., Kennedy, D., Klaveness, S., Montillo, A., Makris, N., Rosen, B., & Dale, A. M. (2002). Whole brain segmentation: Neurotechnique automated labeling of neuroanatomical structures in the human. *Brain*, *33*, 341–355. [https://doi.org/10.1016/s0896-6273\(02\)00569-x](https://doi.org/10.1016/s0896-6273(02)00569-x)
- Fischl, B., Salat, D. H., van der Kouwe, A. J. W., Makris, N., Ségonne, F., Quinn, B. T., & Dale, A. M. (2004). Sequence-independent segmentation of magnetic resonance images. *NeuroImage*, *23*(Suppl 1), S69–S84. <https://doi.org/10.1016/j.neuroimage.2004.07.016>
- Fitzgerald, J. M., DiGangi, J. A., & Phan, K. L. (2019). Functional neuroanatomy of emotion and its regulation in PTSD. *Harvard Review of Psychiatry*, *26*(3), 116–128. <https://doi.org/10.1097/HRP.0000000000000185>
- Gousias, I. S., Edwards, A. D., Rutherford, M. A., Counsell, S. J., Hajnal, J. V., Rueckert, D., & Hammers, A. (2012). Magnetic resonance imaging of the newborn brain: Manual segmentation of labelled atlases in term-born and preterm infants. *NeuroImage*, *62*(3), 1499–1509. <https://doi.org/10.1016/j.neuroimage.2012.05.083>
- Greene, D. J., Black, K. J., & Schlaggar, B. L. (2016). Considerations for MRI study design and implementation in pediatric and clinical populations. *Developmental Cognitive Neuroscience*, *18*, 101–112. <https://doi.org/10.1016/j.dcn.2015.12.005>
- Grimm, O., Pohlack, S., Cacciaglia, R., Winkelmann, T., Plichta, M. M., Demirakca, T., & Flor, H. (2015). Amygdalar and hippocampal volume: A comparison between manual segmentation, Freesurfer and VBM. *Journal of Neuroscience Methods*, *253*, 254–261. <https://doi.org/10.1016/j.jneumeth.2015.05.024>
- Grohs, M. N., Lebel, C., Carlson, H. L., Craig, B. T., & Dewey, D. (2021). Subcortical brain structure in children with developmental coordination disorder: A T1-weighted volumetric study. *Brain Imaging and Behavior*, *15*(6), 2756–2765. <https://doi.org/10.1007/s11682-021-00502-y>
- Hannoun, S., Tutunji, R., El Homsy, M., Saaybi, S., & Hourani, R. (2019). Automatic thalamus segmentation on unenhanced 3D

- T1 weighted images: Comparison of publicly available segmentation methods in a pediatric population. *Neuroinformatics*, 17(3), 443–450. <https://doi.org/10.1007/s12021-018-9408-7>
- Hashempour, N., Tuulari, J. J., Merisaari, H., Lidauer, K., Luukkonen, I., Saunavaara, J., Parkkola, R., Lähdesmäki, T., Lehtola, S. J., Keskinen, M., Lewis, J. D., Scheinin, N. M., Karlsson, L., & Karlsson, H. (2019). A novel approach for manual segmentation of the amygdala and hippocampus in neonate MRI. *Frontiers in Neuroscience*, 13, 1025. <https://doi.org/10.3389/fnins.2019.01025>
- Herrero, M., & Barcia, C. (2002). Functional anatomy of thalamus and basal ganglia. *Child's Nervous System*, 18, 386–404. <https://doi.org/10.1007/s00381-002-0604-1>
- Jaroudi, W., Garami, J., Garrido, S., Hornberger, M., Keri, S., & Moustafa, A. A. (2017). Factors underlying cognitive decline in old age and Alzheimer's disease: The role of the hippocampus. *Reviews in the Neurosciences*, 28(7), 705–714. <https://doi.org/10.1515/revneuro-2016-0086>
- Karlsson, L., Tolvanen, M., Scheinin, N. M., Uusitupa, H., Korja, R., Ekholm, E., Tuulari, J. J., Pajulo, M., Huutilainen, M., Paunio, T., Karlsson, H., & FinnBrain Birth Cohort Study Group. (2018). Cohort profile: The FinnBrain birth cohort study (FinnBrain). *International Journal of Epidemiology*, 47(1), 15–16j. <https://doi.org/10.1093/ije/dyx173>
- Krabbe, S., Gründemann, J., & Lüthi, A. (2018). Review amygdala inhibitory circuits regulate associative fear conditioning. *Biological Psychiatry*, 83(10), 800–809. <https://doi.org/10.1016/j.biopsych.2017.10.006>
- Lee, A., Poh, J. S., Wen, D. J., Tan, H. M., Chong, Y.-S., Tan, K. H., Gluckman, P. D., Fortier, M. V., Rifkin-Graboi, A., & Qiu, A. (2019). Maternal care in infancy and the course of limbic development. *Developmental Cognitive Neuroscience*, 40, 100714. <https://doi.org/10.1016/j.dcn.2019.100714>
- Makowski, C., Béland, S., Kostopoulos, P., Bhagwat, N., Devenyi, G. A., Malla, A. K., Joobar, R., Lepage, M., & Chakravarty, M. M. (2018). Evaluating accuracy of striatal, pallidal, and thalamic segmentation methods: Comparing automated approaches to manual delineation. *NeuroImage*, 170, 182–198. <https://doi.org/10.1016/j.neuroimage.2017.02.069>
- Manes, J. L., Tjaden, K., Parrish, T., Simuni, T., Roberts, A., Greenlee, J. D., Corcos, D. M., & Kurani, A. S. (2018). Altered resting-state functional connectivity of the putamen and internal globus pallidus is related to speech impairment in Parkinson's disease. 8(9), e01073. <https://doi.org/10.1002/brb3.1073>
- McDonald, A. J., & Mott, D. D. (2017). Functional neuroanatomy of amygdalohippocampal interconnections and their role in learning and memory. *Journal of Neuroscience Research*, 95(3), 797–820. <https://doi.org/10.1002/jnr.23709>
- McGraw, K. O., & Wong, S. P. (1996). Forming inferences about some intraclass correlation coefficients. *Psychological Methods*, 1(1), 30–46. <https://doi.org/10.1037/1082-989X.1.1.30>
- Moore, M., Hu, Y., Woo, S., O'Hearn, D., Jordan, A. D., Dolcos, S., & Dolcos, F. (2014). A comprehensive protocol for manual segmentation of the medial temporal lobe structures. *Journal of Visualized Experiments: JoVE*, (89), e50991. <https://doi.org/10.3791/50991>
- Morey, R. A., Petty, C. M., Xu, Y., Pannu Hayes, J., Wagner, H. R., Lewis, D. V., LaBar, K. S., Styner, M., & McCarthy, G. (2009). A comparison of automated segmentation and manual tracing for quantifying hippocampal and amygdala volumes ☆. *NeuroImage*, 45(3), 855–866. <https://doi.org/10.1016/j.neuroimage.2008.12.033>
- Mulder, E. R., de Jong, R. A., Knol, D. L., van Schijndel, R. A., Cover, K. S., Visser, P. J., Barkhof, F., Vrenken, H., & Alzheimer's Disease Neuroimaging Initiative. (2014). Hippocampal volume change measurement: Quantitative assessment of the reproducibility of expert manual outlining and the automated methods FreeSurfer and FIRST. *NeuroImage*, 92, 169–181. <https://doi.org/10.1016/j.neuroimage.2014.01.058>
- Næss-Schmidt, E., Tietze, A., Blicher, J. U., Petersen, M., Mikkelsen, I. K., Coupé, P., Manjón, J. V., & Eskildsen, S. F. (2016). Automatic thalamus and hippocampus segmentation from MP2RAGE: Comparison of publicly available methods and implications for DTI quantification. *International Journal of Computer Assisted Radiology and Surgery*, 11, 1979–1991. <https://doi.org/10.1007/s11548-016-1433-0>
- Nugent, A. C., Luckenbaugh, D. A., Wood, S. E., Bogers, W., Zarate, C. A. Jr., & Drevets, W. C. (2013). Automated subcortical segmentation using FIRST: Test-retest reliability, inter-scanner reliability, and comparison to manual segmentation. 34(9), 2313–2329. <https://doi.org/10.1002/hbm.22068>
- Owens-Walton, C., Jakabek, D., Power, B. D., Walterfang, M., Velakoulis, D., van Westen, D., Looi, J. C. L., Shaw, M., & Hansson, O. (2019). Increased functional connectivity of thalamic subdivisions in patients with Parkinson's disease. *PLoS ONE*, 14(9), e0222002. <https://doi.org/10.1371/journal.pone.0222002>
- Pardoe, H. R., Pell, G. S., Abbott, D. F., & Jackson, G. D. (2009). Hippocampal volume assessment in temporal lobe epilepsy: How good is automated segmentation? *Epilepsia*, 50(12), 2586–2592. <https://doi.org/10.1111/j.1528-1167.2009.02243.x>
- Parnaudeau, S., Bolkan, S. S., & Kellendonk, C. (2018). The medio-dorsal thalamus: An essential partner of the prefrontal cortex for cognition. *Biological Psychiatry*, 83, 648–656. <https://doi.org/10.1016/j.biopsych.2017.11.008>
- Patenaude, B., Smith, S. M., Kennedy, D. N., & Jenkinson, M. (2011). A Bayesian model of shape and appearance for subcortical brain segmentation. *NeuroImage*, 56(3), 907–922. <https://doi.org/10.1016/j.neuroimage.2011.02.046>
- Perlaki, G., Horvath, R., Nagy, S. A., Bogner, P., Doczi, T., Janszky, J., & Orsi, G. (2017). Comparison of accuracy between FSL's FIRST and Freesurfer for caudate nucleus and putamen segmentation. *Scientific Reports*, 7(1), 2418. <https://doi.org/10.1038/s41598-017-02584-5>
- Pipitone, J., Park, M. T., Winterburn, J., Lett, T. A., Lerch, J. P., Pruessner, J. C., Lepage, M., Voineskos, A. N., Chakravarty, M. M., & Alzheimer's Disease Neuroimaging Initiative. (2014). Multi-atlas segmentation of the whole hippocampus and subfields using multiple automatically generated templates. *NeuroImage*, 101, 494–512. <https://doi.org/10.1016/j.neuroimage.2014.04.054>
- Power, B. D., Wilkes, F. A., Hunter-Dickson, M., van Westen, D., Santillo, A. F., Walterfang, M., Nilsson, C., Velakoulis, D., & Looi, J. C. L. (2015). Validation of a protocol for manual segmentation of the thalamus on magnetic resonance imaging scans. *Psychiatry Research*, 232(1), 98–105. <https://doi.org/10.1016/j.psychres.2015.02.001>

- Pulli, E. P., Eero, S., Venla, K., Anni, C., Harri, M., Jani, S., Riitta, P., Tuire, L., Ekaterina, S., Saara, N., Eeva-Leena, K., Riikka, K., Linnea, K., Hasse, K., & Tuulari Jetro, J. (2022). Feasibility of FreeSurfer processing for T1-weighted brain images of 5-year-olds: Semiautomated protocol of FinnBrain neuroimaging lab. *Frontiers in Neuroscience*, *16*, 874062. <https://doi.org/10.3389/fnins.2022.874062>
- Pulli, E. P., Kumpulainen, V., Kasurinen, J. H., Korja, R., Merisaari, H., Karlsson, L., Parkkola, R., Saunavaara, J., Lähdesmäki, T., Scheinin, N. M., Karlsson, H., & Tuulari, J. J. (2019). Prenatal exposures and infant brain: Review of magnetic resonance imaging studies and a population description analysis. *Human Brain Mapping*, *40*(6), 1987–2000. <https://doi.org/10.1002/hbm.24480>
- Reuter, M., Rosas, H. D., & Fischl, B. (2010). Highly accurate inverse consistent registration: A robust approach. *NeuroImage*, *53*(4), 1181–1196. <https://doi.org/10.1016/j.neuroimage.2010.07.020>
- Reuter, M., Schmansky, N. J., Rosas, H. D., & Fischl, B. (2012). Within-subject template estimation for unbiased longitudinal image analysis. *NeuroImage*, *61*(4), 1402–1418. <https://doi.org/10.1016/j.neuroimage.2012.02.084>
- Roediger, D. J., Krueger, A. M., de Water, E., Mueller, B. A., Boys, C. A., Hendrickson, T. J., Schumacher, M. J., Mattson, S. N., Jones, K. L., Lim, K. O., & Wozniak, J. R. (2021). Hippocampal subfield abnormalities and memory functioning in children with fetal alcohol spectrum disorders. *Neurotoxicology and Teratology*, *83*, 106944. <https://doi.org/10.1016/j.ntt.2020.106944>
- Sandman, C. A., Head, K., Muftuler, L. T., Su, L., Buss, C., & Davis, E. P. (2014). Shape of the basal ganglia in preadolescent children is associated with cognitive performance. *NeuroImage*, *99*, 93–102. <https://doi.org/10.1016/j.neuroimage.2014.05.020>
- Sawangjit, A., Oyanedel, C. N., Niethard, N., Salazar, C., Born, J., & Inostroza, M. (2018). The hippocampus is crucial for forming non-hippocampal long-term memory during sleep. *Nature*, *564*(7734), 109–113. <https://doi.org/10.1038/s41586-018-0716-8>
- Schoemaker, D., Buss, C., Head, K., Sandman, C. A., Davis, E. P., Chakravarty, M. M., Gauthier, S., & Pruessner, J. C. (2016). Corrigendum to “Hippocampus and amygdala volumes from magnetic resonance images in children: Assessing accuracy of FreeSurfer and FSL against manual segmentation” [*NeuroImage* 129 (2016) 1–14] (S1053811916000537) (10.1016/j.neuroimage.2016.01.038). *NeuroImage*, *173*, 1–2. <https://doi.org/10.1016/j.neuroimage.2018.02.009>
- Segonne, F., Dale, A. M., Busa, E., Glessner, M., Salat, D., Hahn, H. K., & Fischl, B. (2004). A hybrid approach to the skull stripping problem in MRI. *NeuroImage*, *22*, 1060–1075. <https://doi.org/10.1016/j.neuroimage.2004.03.032>
- Shrout, P. E., & Fleiss, J. L. (1979). Intraclass correlations: Uses in assessing rater reliability. *Psychological Bulletin*, *86*(2), 420–428. <https://doi.org/10.1037//0033-2909.86.2.420>
- Singh-bains, M. K., Waldvogel, H. J., & Faull, R. L. M. (2016). The role of the human globus pallidus in Huntington’s disease. *Brain Pathology*, *26*, 741–751. <https://doi.org/10.1111/bpa.12429>
- Terwee, C. B., Bot, S. D. M., de Boer, M. R., van der Windt, D. A., Knol, D. L., Dekker, J., Bouter, L. M., & de Vet, H. C. (2007). Quality criteria were proposed for measurement properties of health status questionnaires. *Journal of Clinical Epidemiology*, *60*, 34–42. <https://doi.org/10.1016/j.jclinepi.2006.03.012>
- Toazza, R., Franco, A. R., Buchweitz, A., Molle, R. D., Rodrigues, D. M., Reis, R. S., Mucellini, A. B., Esper, N. B., Aguzzoli, C., Silveira, P. P., Salum, G. A., & Manfro, G. G. (2016). Amygdala-based intrinsic functional connectivity and anxiety disorders in adolescents and young adults. *Psychiatry Research: Neuroimaging*, *257*, 11–16. <https://doi.org/10.1016/j.pscychresns.2016.09.010>
- Tye, K. M., Prakash, R., Kim, S., Fenno, L. E., Grosenick, L., Zarabi, H., Thompson, K. R., Gradinaru, V., Ramakrishnan, C., & Deisseroth, K. (2011). Amygdala circuitry mediating reversible and bidirectional control of anxiety. *Nature*, *471*(7338), 358–362. <https://doi.org/10.1038/nature09820>. Amygdala
- Velasco-Annis, C., Akhondi-asl, A., Stamm, A., & Warfield, S. K. (2017). Reproducibility of brain MRI segmentation algorithms: Empirical comparison of local MAP PSTAPLE, FreeSurfer, and FSL-FIRST. 12–15. <https://doi.org/10.1111/jon.12483>
- Wang, Z., Fontaine, M., Cyr, M., Rynn, M. A., Simpson, H. B., Marsh, R., & Pagliaccio, D. (2022). Subcortical shape in pediatric and adult obsessive-compulsive disorder. *Depression and Anxiety*, *39*, 504–514. <https://doi.org/10.1002/da.23261>
- Zou, K., Warfield, S., Bharatha, A., Tempany, C., Kaus, M., Haker, S., Wells, W. M. III, Jolesz, F. A., & Kikinis, R. (2004). Statistical validation of image segmentation quality based on a spatial overlap index. *Academic Radiology*, *11*(2), 178–189. [https://doi.org/10.1016/S1076-6332\(03\)00671-8](https://doi.org/10.1016/S1076-6332(03)00671-8)

SUPPORTING INFORMATION

Additional supporting information can be found online in the Supporting Information section at the end of this article.

How to cite this article: Lidauer, K., Pulli, E. P., Copeland, A., Silver, E., Kumpulainen, V., Hashempour, N., Merisaari, H., Saunavaara, J., Parkkola, R., Lähdesmäki, T., Saukko, E., Nolvi, S., Kataja, E.-L., Karlsson, L., Karlsson, H., & Tuulari, J. J. (2022). Subcortical and hippocampal brain segmentation in 5-year-old children: Validation of FSL-FIRST and FreeSurfer against manual segmentation. *European Journal of Neuroscience*, *56*(5), 4619–4641. <https://doi.org/10.1111/ejn.15761>